Coupling of electrons and intramolecular vibrations in TTF-TCNQ (tetrathiafulvalene-tetracyanoquinodimethane)

Shahab Etemad*
Department of Physics, Sharif University of Technology,† P.O. Box 3406, Tehran, Iran
(Received 11 August 1980)

We report experimental evidence for electron-intramolecular vibration coupling in TTF-TCNQ (tetrathiafulvalene-tetracyanoquinodimethane). Linear coupling of totally symmetric vibrations of a_g modes to the oscillation in the phase of the charge-density waves gives rise to a set of IR-(infrared-) active modes which grow in intensity with the onset of the Peierls transition. Our experimental estimates of electron-intramolecular coupling constants of the TCNQ molecule are in good agreement with previous values. Moreover, the experimentally determined total electron-intramolecular coupling constant is $\lambda \simeq 0.35$ for TCNQ stacks in TTF-TCNQ. These results indicate that the Peierls distorted state is predominantly stabilized by coupling of the unpaired electrons to the intramolecular vibrations. With the onset of Peierls transition, the two IR-active modes of CN-stretching vibration show a splitting due to a shift in frequency of the mode with the dipole component parallel to the crystallographic *b* and *c* axes. The splitting is also seen in the selenium analog TSeF-TCNQ and is consistent with the x-ray diffuse scattering result that the Peierls distortion is due to a rigid molecular translation in the *bc* plane. The temperature dependence of both effects show the presence of the sizable amplitude of the fluctuating charge-density waves in the temperature range $53 < T < 150$ K. This result indicates that the collective contribution to dc conductivity is not limited to a small temperature range just above $T_c \simeq 53$ K. We have also commented on some theoretical points of view using the underlying information in the vibrational spectra of TTF-TCNQ. A preliminary report of the experimental results was given by S. Etemad [Bull. Am. Phys. Soc. 23, 381 (1978)].

I. INTRODUCTION

Considerable progress has been achieved in the past decade in developing an understanding of a variety of phenomena in the one-dimensional (1D) limit of solid-state physics.[1–4] The experimental realizations of these phenomena have been primarily based on a large number of charge-transfer salts of planar donor and acceptor molecules. The charge-transfer salts of interest crystallize in segregated donor and/or acceptor stacks. Their 1D electronic properties primarily arise from the highly anisotropic overlap between the neighboring unpaired π-electron orbitals. They commonly exhibit semiconducting properties at room temperature. This arises from the onset of Peierls[5] distortion at a somewhat higher temperature. Their relatively high Peierls transition temperature is due to the commensurate charge transfer as well as the strong Coulomb potential of the fully ionized strong acceptor or donor present. In several cases, where partial charge transfer prevails, the Peierls transition is suppressed down to subambient temperatures resulting in a metallic state at room temperature and a narrow-gap semiconducting state at $T=0$. In a recent exciting discovery it is shown that under application of hydrostatic pressure a superconducting low-temperature ground state could be energetically more favorable than the Peierls semiconducting state.[6]

By far the most widely studied salt of this category has been tetrathiafulvalene-tetracyanoquinodimethane (TTF-TCNQ).[1–4] TTF-TCNQ crystallizes in segregated stacks of TTF and TCNQ molecules.[7] Its crystal structure is monoclinic with two TTF-TCNQ molecules per unit cell. The molecules stack along the conducting *b* axis with a close interplanar separation of 3.17 and 3.47 Å for TCNQ and TTF, respectively. The neighboring stacks of either kind are tilted in the opposite directions with respect to the conducting *b* axis. The tilt angles are 34° and 24.5° for TCNQ and TTF stacks, respectively.[7] At room temperature TTF-TCNQ is a pseudo-one-dimensional metal with a conductivity of about 500 $\text{cm}^{-1}\ \Omega^{-1}$ along the stacking *b* axis.[8,9] Polarized reflectance measurements show a Drude edge structure only along this axis indicative of 1D electronic band structure which arises from anisotropic overlap of unpaired π-electron orbitals.[10,11] Studies of thermoelectric power measurements in the alloy systems $(\text{TSeF})_x(\text{TTF})_{1-x}$-TCNQ indicates that both chains contribute to the conductivity.[12,13] The strongly-temperature-dependent conductivity appears to be intrinsic[14] to these systems and its origin is still a subject of controversy.

The metallic state of TTF-TCNQ primarily arises from an incomplete charge transfer of $\rho = 0.59$, a

value obtained from the x-ray diffuse scattering measurements.[15] In lowering the temperature a metal-semiconductor (MS) transition occurs at $T_{c_1} \simeq 53$ K. Preceding the MS transition uncorrelated and incommensurate 1D charge-density waves (CDW) of wave vector two and four times the Fermi wave vector k_F have been detected.[15,16] The T_{c1} transition appears to be driven by the three-dimensional (3D) ordering of the $2k_F$ CDW on TCNQ stacks[9,17] resulting in a Peierls distorted semiconducting state for $T < 53$ K. The Peierls gap 2Δ in TTF-TCNQ is relatively small consistent with the low transition temperature. The size of the gap is $2\Delta \simeq 400$ cm^{-1} as determined from the onset of the photoconductivity[18] or from the activation energy for conductivity.[9] The $2k_F$ CDW arises from the opening of the Peierls gap at the Fermi level with the associated softening of phonons at $q = 2k_F$. The one-dimensionally-ordered $2k_F$ CDW's start to appear at $T_{MF} \simeq 150$ K, the mean-field transition temperature. In the temperature region $T_{c_1} < T < T_{MF}$ the collective incommensurate sliding CDW appears to act as a vehicle for the electrons to augment their single-particle conductivity.[19,20]

The strong electron-phonon coupling in TTF-TCNQ does not arise from coupling of the electrons to only the acoustic phonons. The delocalized unpaired π electrons appear to have a sizable coupling to most of the intramolecular vibrational modes. Due to the large numbers of such modes their total coupling constant to the π electrons is considerably larger than that of the acoustic phonons. In this context, it has been suggested that the Peierls distorted state may, in fact, be primarily stabilized by an appropriate combination of molecular and lattice distortions.[21] The theoretical estimate of total π-electron-intramolecular-vibrational (EIMV) coupling constant in TCNQ stacks of TTF-TCNQ is large and supports this point of view.[22] These coupling constants have been also determined by studies of infrared (ir) spectrum of several TCNQ compounds by Rice and co-workers.[23–25] All these compounds have a relatively large semiconducting gap and are already in their Peierls distorted state at room temperature. The EIMV coupling in these compounds gives rise to a series of new IR-active modes that will be referred to as "vibronic modes" in this work. These modes arise from the first-order coupling of the totally symmetric a_g vibrational modes of TTF and TCNQ molecules to oscillation in phase of the CDW along the stacks.[26,27] The EIMV coupling constants in these compounds have been determined from an analysis of the frequency of the vibronic modes compared to that of their associated totally symmetric a_g modes. Despite the great interest in TTF-TCNQ a study of EIMV in this system has not been carried out. The reported works[28–30] on studies of the vibrational modes of TTF-TCNQ in the IR region have clearly fallen short of this task.

In this work we present the first detailed experimental evidence for EIMV coupling in TTF-TCNQ achieved by studying its vibrational spectrum in the IR region as a function of temperature. Using the temperature dependence of the vibronic modes we have monitored the growth of the $2k_F$ CDW amplitude as the temperature is lowered below the Peierls transition. The values of EIMV coupling constants estimated for TCNQ molecule in TTF-TCNQ are in agreement with those found in the other TCNQ compounds by Rice and co-workers.[23–25] Due to the small size of the Periels gap in TTF-TCNQ most of the vibronic modes lie in the range above the gap.[9,18] This has enabled us to determine the total electron-phonon coupling constant for the TCNQ stacks. Besides the first-order coupling of the CDW to the a_g modes we have also discovered that some normally IR-active modes do couple to the CDW. In particular, the two IR-active modes of the four CN groups at the corners of the TCNQ molecules show a splitting due to the shift in frequency of the mode with dipole components parallel to the crystallographic b and c axes. The splitting is in agreement with the recent finding that the Peierls distortion is due to rigid molecular translations in the bc plane. The resulting temperature dependence of the frequency of this mode appears to provide a reasonably accurate temperature dependence of the CDW amplitude. These results are presented in Sec. II. In Sec. III we present a synopsis of EIMV coupling, analysis of the vibronic modes, a discussion of anomalous EIMV, and a general discussion of the results. Concluding remarks are presented in Sec. IV.

II. EXPERIMENTAL PROCEDURES AND RESULTS

The physical properties of TTF-TCNQ have caused considerable difficulty in choosing an appropriate sample configuration for studying its vibrational spectrum. For single-crystal studies, in particular the small size and the high absorption coefficient have been the limiting factors in obtaining a high signal-to-noise ratio. The high absorption coefficient in the region of the vibrational frequencies results from the small size of the optical gap, $2\Delta \simeq 400$ cm^{-1}, in the absorption spectrum.

In the present work the study of the vibrational spectrum has primarily been carried out in the transmission mode on polycrystalline samples dispersed in a KBr matrix. To ensure that the vibrational spectra are not unacceptably affected by the presence of the KBr matrix the absorption spectra have been compared against the reflection spectra from a compaction of single crystals. We note that the absorption coefficients parallel and perpendicular to the b axis are about 10^5 and 10^4 cm^{-1}, respective-

ly.[11] As a result the transmission through a microcrystal, dispersed randomly in the KBr matrix, shows the *b*-axis polarization of a vibrational mode only if its thickness is a few tenths of a μ or smaller. The *a*- and *c*-axes polarization of a mode can be detected for microcrystal thickness of up to a few μ.[30] Thicker microcrystals are opaque.

The TTF-TCNQ crystal used for the transmission studies were grown by the standard technique of slow diffusion of TCNQ and TTF in acetonitrile solution. Small single crystals of TTF-TCNQ were grown overnight. We note that for these studies sample quality was not as critical as in transport measurements.[8,9] Samples for the transmission studies were prepared by crushing, gently and extensively, about 0.5–1.0 mg per $\frac{1}{2}$-in. pellet of small single crystals together with KBr powder in an agate mortar. Some degree of control on the size distribution of the microcrystals could be exerted by varying the crushing time. A substantial fraction of microcrystals in most samples was thin enough for studying the *b*-axis component of the vibrational modes. The mixture was finally pressed to form a uniformly tinted transparent pellet.

The spectra presented in this work were taken on a Perkin-Elmer 580 spectrophotometer. A modified Air Products CSA202 closed cycle refrigerator was used together with a Lake Shore Cryogenics DTC-500 temperature controller for collecting the spectra at subambient temperatures. To measure the temperature a calibrated GaAs diode was incorporated in a HCOF (high-conductivity oxygen-free) copper block, in which the pellets were framed using Cry-Con conducting grease.

The transmission spectra of TTF-TCNQ in the range 250–4000 cm^{-1} are shown in Figs. 1 and 2 for two representative samples. Figure 1 shows the variation of the transmission spectra over a wide energy range, while Fig. 2 covers the energy range where

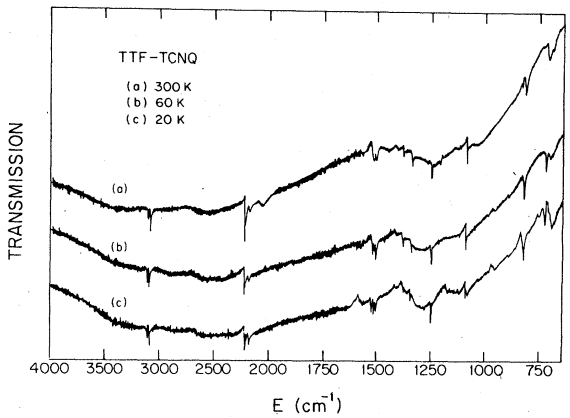

FIG. 1. Transmission spectra of TTF-TCNQ in the range from 700 cm^{-1} for $T = 300$, 60, and 20 K.

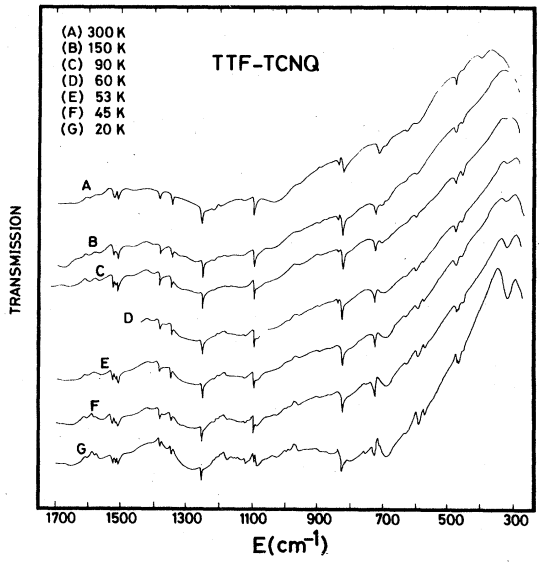

FIG. 2. Transmission spectra of TTF-TCNQ in the region of the vibrational modes for several temperatures.

most of the vibrational modes lie. The temperatures shown in Fig. 2 were chosen to emphasize the transition region. The low-energy side of the spectra are cut off because of the strong KBr absorption centered at lower frequencies. The absolute value of transmission does not change much over the whole energy range. In the room-temperature trace in Fig. 2, for example, the transmission changes from a value of 17% at 1750 cm^{-1} to a maximum of 27% at 380 cm^{-1}. The values of transmission at the two limits depend on the amount as well as the size distribution of the crushed sample particles in the pellet.

The room-temperature spectra shown in Figs. 1 and 2 show several sharp minima in transmission, related to the characteristic infrared-active vibrational modes of TTF and TCNQ molecules, spread over a smoothly varying background. A complete assignment of these modes will not be attempted in this work. However, the two well-separated structures at about 2200 and 3100 cm^{-1}, belonging to the CN and CH stretching modes, respectively, will be discussed further.

A significant result is the change in the transmission spectra as samples are cooled below the Peierls transition temperature of TTF-TCNQ. Of principal importance is the appearance of a new set of structures as the Peierls distortion sets in. These new structures are characterized by *peaks* in transmission preceded by minima of comparable width on their low-energy side.[31] The energy, ω_n^{ϕ}, and width, $\delta\omega_n^{\phi}$, of these structures are tabulated in Table I. The frequencies of these structures appear to be related to the frequencies of some of the totally symmetric a_g

TABLE I. The frequency (ω_ϕ) and width ($\delta\omega_\phi$) of the a_g modes of TTF-TCNQ that have IR activity in the Peierls distorted state. ω_0 is the unperturbed zone-center frequency measured by Raman spectroscopy.

a_g mode	ω_ϕ (cm^{-1})	$\delta\omega_\phi$ (cm^{-1})	ω_0 (cm^{-1})[a]
Q_2			2215
Q_3	1580	50	1604
Q_4	1385	30	1423
Q_5	1185	20	1200
Q_6	975	20	1000
Q_7			712
Q_8	595	15	600[b]
Q_9	320	20	332
F_2			1515
F_3	1400	100	1454
F_4	1095	10	
F_5	725	30	746
F_6	350	50	500

[a]From Temkin and Fitchen, Ref. 32. [b]From Kuzmany and Stoltz, Ref. 33.

modes of TTF-TCNQ. In the other column in Table I we have reproduced these frequencies, measured by Raman spectroscopy, for comparison.[32,33] Our assignment of Raman lines to a_g modes of TCNQ and TTF is by comparison with the a_g modes assignments in TTF^0 and $TCNQ^0$ and in their radical ions. For example the 1454-cm^{-1} Raman line has been previously assigned to $a_g(Q_4)$.[32,33] Noting that the frequency of this mode varies from 1454 cm^{-1} in $TCNQ^0$ to 1391 cm^{-1} in $TCNQ^-$ makes the assignments of Table I more appropriate. Instead we have assigned the 1454-cm^{-1} line to $a_g(F_3)$. The frequency of this mode varies from 1518 cm^{-1} in TTF^0 to 1420 cm^{-1} in TTF^+.

The most apparent low-temperature structure is a 60-cm^{-1} wide peak at 350 cm^{-1} shown in more detail in the inset of Fig. 3. The broad minimum preceding the peak appears to have a somewhat sharper, 20-cm^{-1} wide, transmission minimum superimposed on it. The sharper minimum centered at 320 cm^{-1} appears to have a similar temperature dependence as the peak. Their temperature dependence, shown in Fig. 3, is representative of all of the new structures presented in Table I. We note that the fastest rate of growth for these structures coincides with the Peierls transition temperature at 53 K.[9] The intensity of these structures seem to decrease rather slowly as the temperature is raised above 53 K. This behavior should be contrasted with the sudden disappearance of the superlattice satellite intensities associated with the three-dimensional phase transition at 53 K.[34]

Another significant result is seen in the temperature dependence of the characteristic CN-stretching vibration of TCNQ molecule shown in Fig. 4. At room temperature this structure contains the most intense absorption line of the spectrum at 2216 cm^{-1}. The apparent distortion in the shape of this line at room temperature is due to the presence of KBr matrix. This is due to the so-called Christiansen effect which arises from the competition between the in-

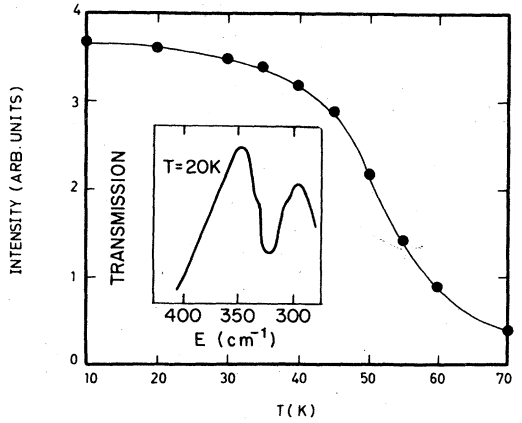

FIG. 3. Temperature dependence of the intensity of the vibronic mode associated primarily with $a_g(F_b)$ of the TTF molecule. Inset shows the transmission spectrum at $T=20$ K detailing this vibronic mode.

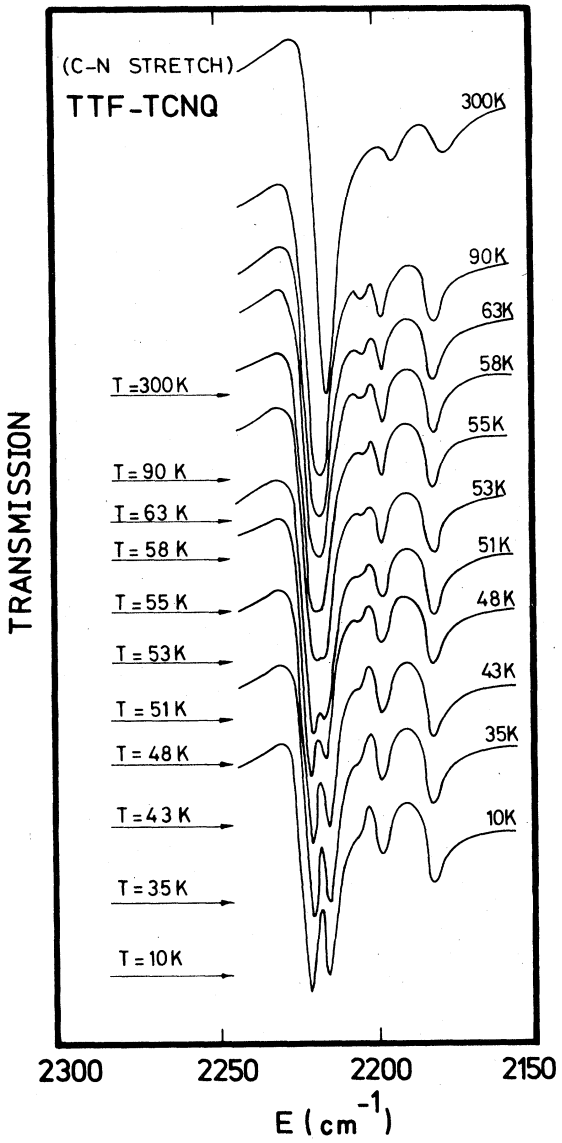

FIG. 4. Temperature dependence of the CN-stretching mode.

dices of refraction of KBr and TTF-TCNQ near a sharp absorption line.

At the lowest temperature in Fig. 4 the intense CN-stretching line is clearly seen to be split into two lines at 2222 and 2216 cm^{-1}. The splitting is gradual, affecting the line by broadening it first. This can be seen in the trace taken at 90 K in which the line is broadened, instead of being narrowed due to lowering of the temperature, and has shifted to 2218 cm^{-1}. The line broadening becomes detectable at about 150 K, close to the temperature where the $2k_F$ streaks appear in the x-ray diffuse scattering results.[16] An estimate of the splitting for the unresolved traces of Fig. 4 can be found by fitting the trace to two lines of the same width as in the room-temperature line. The temperature dependence of the splitting is then plotted in Fig. 5. We note that the sharp rise in splitting occurs at the Peierls transition temperature.[9]

Figure 6(a) shows the result of polarized reflectivity measurement at 20 K in the region of the CN-stretching mode of TTF-TCNQ. The sample used was an oriented mosaic of single crystals laid down on their flat *ab* face. The unpolarized trace in Fig. 6(a) shows the two split lines seen in the absorption data of Fig. 4 in the same temperature range. The important result is that the two lines appear to have two different polarizations. The 2222-cm^{-1} line appears to have no component parallel to *b* axis, and the 2216-cm^{-1} line has no component parallel to *a* axis. No information on the component of the vibration parallel to the *c* axis can be obtained with this arrangement.

Figure 6(b) shows room-temperature traces in the same frequency range as in Fig. 6(a). The width of the single line, taken as the width of the region where the reflectivity rises rapidly, is less than 2 cm^{-1} which is close to the instrumental resolution. It, therefore, appears that the unresolved modes seen as a single absorption at 2216 cm^{-1} are degenerate at room temperature. The degeneracy is removed at lower temperatures when the mode with no component parallel to the *a* axis shifts to a lower frequency.

The temperature dependence of the CH-stretching

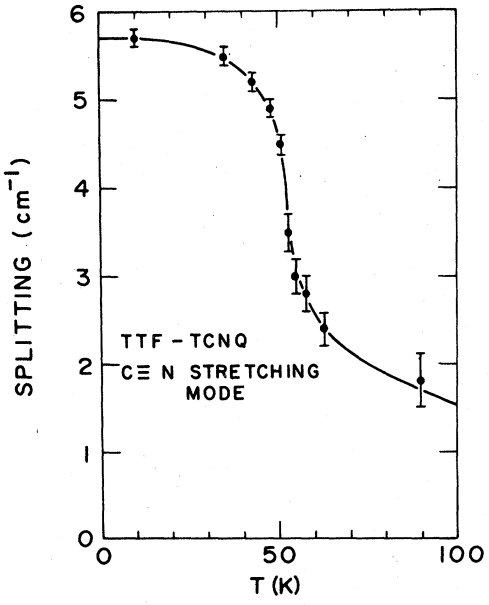

FIG. 5. Temperature dependence of the splitting of the two IR-active modes associated with the CN-stretching vibration.

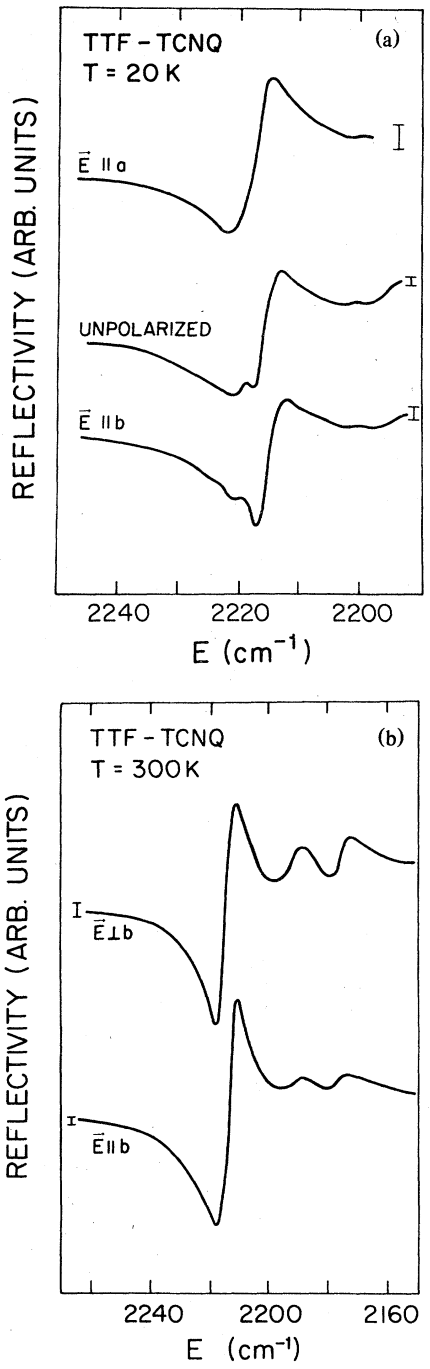

FIG. 6. Polarized reflectivity of the CN-stretching modes; (a) at $T=20$ K, (b) at $T=300$ K.

vibrational mode is shown in Fig. 7. No detectable change in the frequency or the width of the two lines is observed from 10 to 300 K. This behavior can be contrasted with the changes seen in the CN-stretching vibration as a function of temperature, (see Fig. 4).

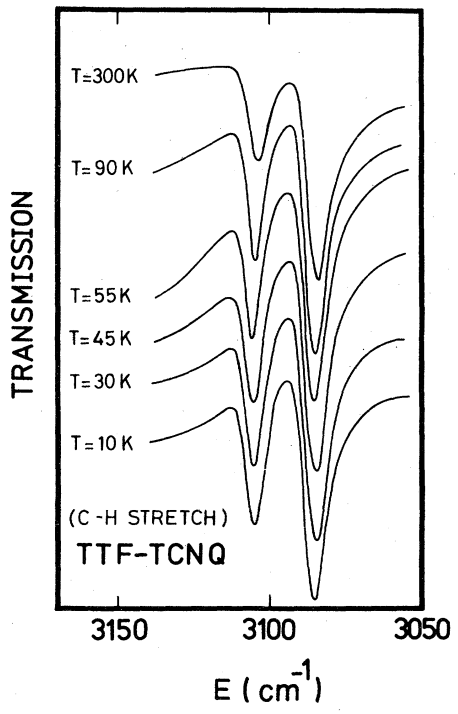

FIG. 7. Temperature dependence of the CH-stretching mode.

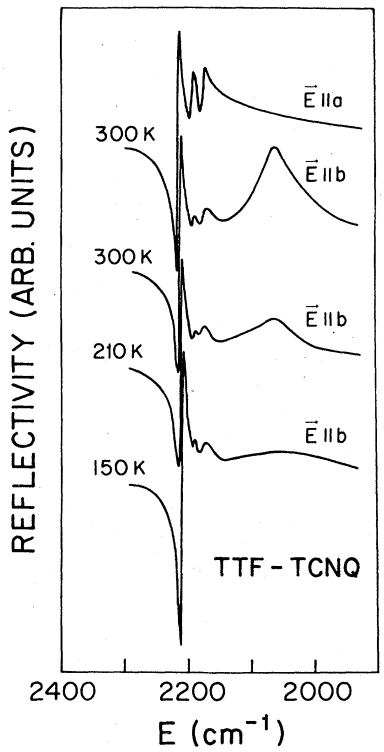

FIG. 8. Polarized reflectivity in the vicinity of the CN-stretching modes for $T=300$, 210, and 150 K.

The polarized reflectivity from 1900 to 2300 cm^{-1} is shown in Fig. 8 as a function of temperature. The result of interest is a strong absorption seen at about 2050 cm^{-1} at 300 K. The absorption has a width of about 80 cm^{-1} and is primarily polarized parallel to the b axis. The temperature dependence of the intensity of this absorption band is complementary to that of the effects already discussed in Figs. 3 and 5. The functional form of the variation in intensity of the structure in Fig. 8 with temperature cannot be obtained unambiguously due to the limited data available. We note that the frequency of this structure is relatively close to that of the CN-stretching vibration, as clearly seen in the room-temperature trace of Fig. 1. It is, therefore, reasonable to associate this structure with the CN-stretching mode.

III. DISCUSSION

A. Electron-intramolecular-vibration coupling

The electron-intramolecular-vibration (EIMV) coupling in TCNQ salts can be simply realized by the following consideration, first noted by Gutfreund *et al.*[35] In order to accommodate the extra electron in going from $TCNQ^0$ to $TCNQ^-$ all bond lengths change, but the change preserves the molecular symmetry. As a result, if the amount of extra charge on a TCNQ molecule is modulated at ω^0, the frequency of a totally symmetric a_g normal mode of vibration, that particular a_g mode would be excited. Inversely if an a_g mode of a TCNQ molecule is excited optically the extra charge on it would be modulated at ω^0, provided that a mechanism for charge transfer exists. Gutfreund *et al.* then argued that the dimensionless electron-intramolecular-vibrational coupling, λ_n, for the nth mode may simply be estimated from

$$\lambda_n \simeq |\psi_n|^2 (\delta R)^2 M \omega_n^{02} N(E_F) \ ,$$

where $|\psi_n|^2$ is the density of the extra electron on the relevant bond, δR is the change in the bond length as one electron is added to the molecule, $M\omega_n^{02}$ is the force constant for the bond, and $N(E_F)$ is the electronic density of states. They suggested a large coupling constant of $\lambda_2 \simeq 0.3$ for the a_g mode which has primarily a CN-stretching characteristic.[35] This is about an order of magnitude larger than its real value as found in a more rigorous treatment of the problem outlined below.

A more rigorous theoretical treatment of the electron-intramolecular-vibration coupling (EIMV) in organic conductors, in particular in TTF-TCNQ, is given in several works by Rice and co-workers.[21–27] Lipari *et al.* noted that the predominant mechanism for EIMV interaction is through the modulation of the energy, E_i, of the molecular-orbital (MO) state which contains the conduction electron.[27] This interaction would lead to a linear EIMV coupling provided that the irreducible representation Γ_i of the electronic state is contained in the direct product of Γ_i and Γ_n, Γ_n being the irreducible representation of the nth normal mode of vibration. Γ_i and Γ_n represent the molecular point groups. Since both TCNQ and TTF molecules have no degenerate electronic states, Lipari *et al.* pointed out that in TTF-TCNQ only the totally symmetric a_g modes contribute to a linear EIMV coupling. Keeping the linear terms in the expansion of the MO energy E_i in terms of the dimensionless normal-mode coordinates, Q_n, would result in[27]

$$E_i(Q_n) = E_i(0) + \sum_n \left(\frac{\partial E_i}{\partial Q_n}\right) Q_n \ . \tag{1}$$

Q_n's are related to the mass-weighted coordinate of atomic displacements in the nth normal mode. The energy of vibration of the nth normal mode is simply given by $\frac{1}{2}\hbar\omega_n^0(Q_n^2 + \dot{Q}_n^2)$ resulting in the vibrational contribution to the Hamiltonian of the form

$$H_{\text{ph}} = \sum_n \sum_q \hbar\omega_n(q)[b_n^\dagger(q) b_n(q) + \tfrac{1}{2}] \ , \tag{2}$$

where $b_n^\dagger$ (b_n) create (annihilate) an optical phonon (intramolecular vibration) of wave vector q, and are related to Q_n by $Q_n(q) = b_n(q) + b_n^\dagger(-q)$. From Eq. (1) the EIMV coupling is then of form $g_n Q_n(q)\rho(-q)$, where the EIMV coupling constant is

$$g_n = \left(\frac{\partial E_i}{\partial Q_n}\right) \ . \tag{3}$$

The operator $\rho(q) = \sum_k a^\dagger(k) a(k+q)$ creates an electronic density fluctuation of wave vector q. $a^\dagger(a)$ is an electron creation (annihilation) operator. The resultant contribution of EIMV coupling to the Hamiltonian is then

$$H_{e\text{-ph}} = \frac{1}{\sqrt{N}} \sum_n \sum_q g_n [b_n(q) + b_n^\dagger(-q)]\rho(-q) \ . \tag{4}$$

In a theoretical model calculation Rice has studied the effect of EIMV on a system of one-dimensional (1D) conduction electrons by considering the total Hamiltonian H

$$H = H_e + H_{e\text{-ph}} + H_{\text{ph}} \ , \tag{5}$$

where H_{ph} and $H_{e\text{-ph}}$ are modified to take into account the contributions from acoustic phonons. H_e is

$$H_e = \sum_k \epsilon_k a_k^\dagger a_k + V[\rho(2k_F) + \rho(-2k_F)] \ , \tag{6}$$

i.e., the electronic contribution to the Hamiltonian describes a system of 1D conduction electrons moving in a periodic potential $V(2k_F)$ of wave vector $2k_F$, twice the Fermi wave vector. The action of V

induces the conduction electrons to form a charge-density wave of wave vector $2k_F$. That in turn opens a Peierls gap of 2Δ at the Fermi level resulting in a semiconducting state. Motivated by the result of the anomalous IR activity in the triethylamnonium salt TEA(TCNQ)$_2$ chain system Rice[26] considers a fixed phase for V with respect to the lattice. This in turn fixes the phase of the CDW's. The CDW field through $H_{e\text{-ph}}$ induces a periodic distortion in the molecular lattice. Thus, the expectation value of $Q_n(q)$ becomes nonvanishing for $q = \pm 2k_F$. As a result the CDW state is further stabilized by the molecular distortion which it initiated.

A most significant result of EIMV coupling manifests itself in the appearance of a new set of IR-active modes polarized parallel to the chain axis. These modes arise from the collective oscillations in the phase of the combined lattice and CDW about their zero equilibrium value.[26] Such oscillations involve a bodily displacement of the CDW and are, therefore, optically active along the chain direction. The optical oscillator strengths involved are electronic rather than ionic in origin, hence they may be quite substantial. Collective oscillations in amplitude of the same modes also give rise to a new set of Raman-active modes with oscillator strengths of the same nature. These Raman-active modes correspond to collective oscillations with wave vector $2k_F$ and should not be confused with the usual zone-center a_g modes. The observation of Temkin and Fitchen that there is not a strong temperature dependence in their Raman spectra of the a_g modes indicates that they are the usual zone-center modes, not the amplitude vibronic modes.[32]

The frequencies of new IR-active modes are close to those of the totally symmetric (a_g) modes which, in the isolated molecule, are not infrared active. The shift in frequency of each collective IR oscillation from that of the a_g mode responsible for it depends primarily on the EIMV coupling constant g_n. For $\omega_n^0 < 2\Delta$, where decay of a collective mode via electron-hole pair excitation is not possible, these modes show up as a series of sharp absorption bands. For $\omega_n^0 > 2\Delta$ these modes are damped by electron-hole pair excitation and would give rise to indentations in the adsorption envelope. Horovitz *et al.*, who have carried out an independent calculation with emphasis on the $\omega_n^0 > 2\Delta$ range, show that the width of such indentations is about $\lambda_n\omega_n$.[36] The dimensionless EIMV coupling, λ_n, is related to g_n in Eq. (3) via $\lambda_n = g_n^2 N(E_F)/\omega_n^0$.

Rice and his collaborators have applied his model calculations,[26] or a modified version of it relevant to the case where charge motion is primarily intradimer oscillation, to TEA-(TCNQ)$_2$,[23] the *N*-methyl-*N*-ethylmorpholinium salt MEM-(TCNQ)$_2$,[25] and the potassium salt K-TCNQ.[24] In these single-chain compounds they successfully manage to produce the most accurate experimental determination of the EIMV coupling constants yet attempted for TCNQ. From their results one would expect in TTF-TCNQ a value in the range 0.02–0.05 for λ_2 compared to $\lambda_2 \simeq 0.3$ based on simple arguments.[35]

In TTF-TCNQ, as can be seen in Figs. 1 and 2, the vibronic modes are considerably weaker than those seen in the dimeric compounds. This is due to the small amplitude of the CDW, a result of a weak initial distortion potential V. In their assignment we have relied on, (1) the variation of their intensity with temperature, (2) the proximity of their frequencies to their associated a_g modes, and (3) their width which should be of order of $\delta\omega_n \simeq \lambda_n\omega_n^0$.[36] In order to find λ_n's and the total electron-phonon coupling constant, $\lambda = \sum_m \lambda_n$, we use Eqs. (6) and (7) of Rice[26] in the limit of weak initial distortion, $V \ll 2\Delta$, i.e.,

$$\sum_n \frac{\lambda_n}{\lambda} \frac{\omega_n^{02}}{\omega_n^{02} - \omega_\phi^2} = \frac{1}{1 + \lambda\tilde{\omega}^2 f_1(\omega)} , \tag{7}$$

where $\tilde{\omega} = \omega^0/2\Delta$ and $f_1(\omega)$ the real part of the function $f(\omega)$ defined as

$$f(\omega) = \frac{\pi i + \ln[(1-s)/(1+s)]}{2s\tilde{\omega}^2} ,$$

with $s = (1-\omega^{-2})^{1/2}$. The solutions of the set of coupled equations in (7) are ω_ϕ's, the frequencies of the vibronic modes. For $\lambda_n \ll \lambda$, as is the case for TCNQ molecule with ten a_g modes, to the first order in λ_n's, the set of equations in (7) decouple to give

$$\frac{\omega_n^0 - \omega_n^\phi}{\omega_n^0} \simeq \frac{\lambda_n}{2}\left[\frac{1}{\lambda} + F(\tilde{\omega}_n)\right] , \tag{8}$$

where $F(\tilde{\omega}_n) = \tilde{\omega}_n^2 f_1(\omega)$ and is plotted as a function of $\tilde{\omega}$ in Fig. 9. λ_n's can then be determined using the experimental values for ω_n^0 and ω_n^ϕ with λ as the single adjustable parameter.

The upper part of Fig. 9 covers the vibronic modes inside the gap, i.e., $\omega_n^0 < 2\Delta$. This is the region where most of the a_g modes of the TCNQ molecule in the compounds studied by Rice and co-workers are situated.[23–25] In TTF-TCNQ the only mode we can observe in this region is the $a_g(Q_9)$ at $\omega_9^\phi = 320$ cm^{-1}. This mode is shifted down from $\omega_9^0 = 332$ cm^{-1}, the original zone-center Raman-active mode of TTF-TCNQ (see Table I). Because $F(\tilde{\omega}_n)$ is positive in this region $(\omega_n^0 - \omega_n^\phi)$ is always positive and not very sensitive to the variation in the value of λ. For example, a variation in the total electron-phonon coupling constant of the TCNQ stacks from $\lambda = 0.3$ to 0.4 in Eq. (8) changes the calculated value of λ_9 from $\lambda_9 = 0.016$ to 0.019, respectively.

In the lower part of Fig. 9 we show the variation of $F(\tilde{\omega}_n)$ for the vibronic modes in the region $\omega_n^0 > 2\Delta$. This is the region where most of the vibronic modes of TTF-TCNQ are situated. We note that in contrast

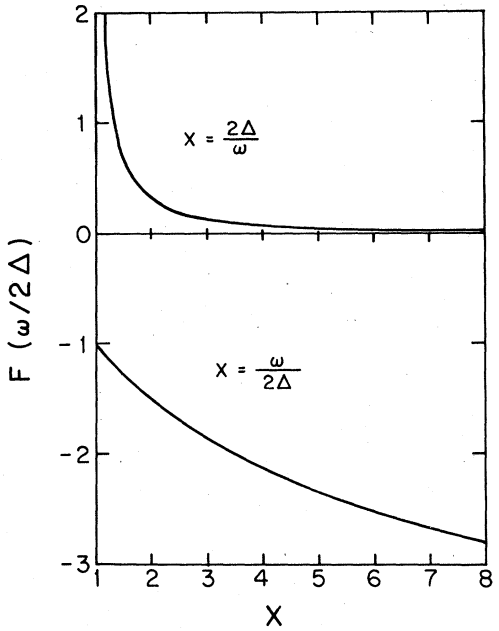

FIG. 9. Dependence of $F(\tilde{\omega}) = \tilde{\omega}^2 f_1(\tilde{\omega})$ on $\tilde{\omega} = \omega/2\Delta$, see Eq. (8).

to the previous case $F(\tilde{\omega}_n)$ is negative in this range, and has a comparable value to that of λ^{-1} for the TCNQ chains. As a result, the experimental determination of λ_n's in this region depend critically on the exact choice of λ. For an a_g mode in this range, depending on its frequency relative to the gap energy, its vibronic counterpart can be at a lower or higher frequency.

Using Eq. (8) and the data of Table I we have calculated the value of the EIMV coupling constants for the a_g modes of TCNQ in TTF-TCNQ as a function of λ. We find that for $\lambda > 0.4$ the self-consistency equation $\lambda = \sum_n \lambda_n$ is violated. For $\lambda < 0.3$, on the other hand, the intrinsic EIMV coupling constants, i.e., g_n's, become too small compared to those values found for the other three TCNQ compounds. The best agreement with the previous results[23–25] is with $\lambda \simeq 0.35$ for the TCNQ stacks in TTF-TCNQ. For this value of λ the experimentally determined dimensionless and intrinsic EIMV coupling constants, λ_n's and g_n's, respectively, of TCNQ stacks are presented in Table II. In order to calculate g_n's from λ_n's we have used $N(E_F) \simeq 2.5$[13] states/eV, appropriate for a tight-binding band structure with a transfer integral $t_Q \simeq 1200$ cm^{-1} and a band filling of $\rho = 0.59$. The other columns of the table show for comparison the intrinsic EIMV coupling constants reproduced from the previous studies of Rice and co-workers.[23–25]

The lack of completeness in determining all of the EIMV coupling constants of TCNQ in TTF-TCNQ is because of the following reasons. The vibronic mode of $a_g(Q_1)$ which should be around 3100 cm^{-1} is usually undetectable due to its very small coupling constant to the CDW's.[23,24] The vibronic mode of $a_g(Q_2)$ is expected to have a sizable $\lambda_2 \simeq 0.03$, estimated by using the values of g_2 from previous studies. Using Eq. (8) the frequency of this vibronic mode is not expected to shift much from $\omega_2^0 \simeq 2220$ cm^{-1}, and is, therefore, hidden underneath the strong ordinarily-IR-active modes of the CN-stretching vibration (see Fig. 4). The vibronic mode of $a_g(Q_7)$ is expected to shift down slightly from $\omega_7^0 \simeq 712$ cm^{-1}. The considerably stronger vibronic mode of $a_g(F_4)$ of the TTF molecule at about 725 cm^{-1}, however, overshadows that of $a_g(Q_7)$ (see Figs. 1 and 2). Finally the frequency of $a_g(Q_{10})$ is outside the range of the present study.

A rough estimate of λ_0, the coupling constant of the electrons to the acoustic phonons, can be ob-

TABLE II. The electron-intramolecular-vibration coupling constants for TCNQ molecules.

Mode	TTF-TCNQ λ	TTF-TCNQ g_n (cm^{-1})	K-TCNQ[a] g_n (cm^{-1})	TEA-(TCNQ)$_2$[b] g_n (cm^{-1})	MEM(TCNQ)$_2$[c] g_n (cm^{-1})
Q_2	(0.025)	(430)	589	339	350
Q_3	0.041	460	670	524	540
Q_4	0.057	510	573	419	500
Q_5	0.025	310	331	323	300
Q_6	0.044	380	339	194	85
Q_7	(0.014)	(180)	169	177	190
Q_8	0.011	146		105	50
Q_9	0.017	140	177	234	180

[a]From Rice, Lipari, and Strassler, Ref. 24.
[b]From Rice, Pietronero, and Bruesch, Ref. 23.
[c]From Rice, Vartsev, and Jacobsen, Ref. 25.

tained by the following considerations. Since g_n is an intrinsic property of the TCNQ molecule we can assume, to a first approximation, that its value is independent of the environment in which a TCNQ molecule lies. This is a reasonable approximation as can be seen by the comparison of the results in Table II. We have, therefore, used the average value of g_n from previous measurements as its representative value for the undetected vibronic mode in TTF-TCNQ. These results are shown in parentheses for $a_g(Q_2)$ and $a_g(Q_7)$ in Table II. The total EIMV coupling constant for the TCNQ molecule in TTF-TCNQ thus is about 0.25. Subtracting this value from $\lambda \simeq 0.35$ results in a rough estimate for the coupling constant of the electrons to the acoustic phonons, i.e., $\lambda_0 \simeq 0.1$.

The relative success of the above analysis is partially due to the small EIMV coupling constant for the individual vibronic modes of the TCNQ molecule. This is not the case for the TTF molecule. A theoretical,[22] as well as an experimental, estimate of λ_n's using $\lambda_n' \simeq \delta\omega_\phi/\omega_\phi$ (Ref. 35) agrees with a very strong EIMV coupling in TTF molecule. The strongest vibronic features detected in TTF-TCNQ at about $\omega_6' = 350$ cm^{-1} and $\omega_3' = 1400$ cm^{-1} are associated with the TTF molecule with estimated dimensionless coupling constants of $\lambda_6' \simeq 0.3$ and $\lambda_3' \simeq 0.2$, respectively.[22] In such strong-coupling regimes the vibronic modes are not independent of each other. In other words their strong coupling to the CDW provides a mechanism for their interaction. As a result, the interaction between two strongly coupled vibronic modes would shift their frequency considerably so that the use of Eq. (8) would be meaningless. Nonetheless, as seen in Figs. 1 and 2 and summarized in Table I the frequency of the observed vibronic modes of the TTF molecule are in qualitative agreement with their expected value.

The temperature dependence of the vibronic modes reveals important information about the growth of the CDW amplitude with decreasing temperature. In Fig. 3 the temperature dependence of the intensity of the vibronic mode associated with $a_g(F_4)$ of the TTF molecule is shown. This vibronic structure shows up as a peak at $\omega_\phi' \simeq 350$ cm^{-1} in the transmission spectrum as seen in the inset to Fig. 3. This structure has red-shifted by about 150 cm^{-1} from its unperturbed zone-center mode at $\omega_0' \simeq 500$ cm^{-1}.[32,33] The large shift in its frequency as well as the relatively large oscillator strength is due to its large EIMV coupling constant.[22] The temperature dependence of the intensity of the vibronic mode has its fastest rate of change at a temperature of about 50 K concurrent with the Peierls transition temperature in TTF-TCNQ. In this context, since the vibronic modes of each molecule are primarily coupled to the CDW on its own segregated stack, such a measurement should in principle be able to show the onset of the Peierls transition on that stack. The uncertainty in these data, however, does not allow a distinction between the Peierls transitions on TCNQ stacks at $T_c \simeq 53$ K (Ref. 9) and on TTF stacks at $T_c' \simeq 49$ K.[37]

The temperature independence of the frequency of the vibronic structures indicates that the a_g modes couple to the uncorrelated 1D CDW above the temperature for 3D ordering in the same manner as they couple to the three-dimensionally-ordered CDW. This is expected because in the time scale of a molecular vibration the sliding incommensurate CDW appears to be stationary. As a result the position of the vibronic structure should not change as the system undergoes Peierls transition. This indeed is reflected in Rice's treatment of the EIMV coupling and is shown by the absence of CDW amplitudes in Eq. (7).[22]

The intensity of a vibronic mode, on the other hand, is closely associated with the amplitude of the CDW to which it is coupled. In the Peierls distorted state the amplitude of the CDW, at a given point has a nonvanishing mean value. For $T < T_c'$ the temperature dependence of the vibronic mode shown in Fig. 3 then reflects the temperature dependence of the Peierls order parameter. In the regime where there are fluctuating uncorrelated CDW's the amplitude of the CDW has a vanishing mean value. In this case the intensity of the vibronic mode reflects the root-mean-square (rms) value of the CDW amplitude. The sizable intensity relative to $T = 0$ of the vibronic structure of Fig. 3 at temperatures well above the 3D transition temperature indicate the rms value of the CDW amplitude is quite large in this temperature regime. The slow decrease with the increase in temperature for $T > T_c$ as seen in Fig. 3, and in Fig. 5 for the anomalous EIMV coupling discussed below, indicate that rms amplitude of the CDW stay large for temperatures as high as $T = 150$ K. This shows that the contribution of the sliding CDW to the dc conductivity is not limited to a small temperature range just above the Peierls transition, consistent with the recent measurements of Andrieux *et al.*[20] that show the sliding mode contribution to the conductivity is observable up to temperatures as high as 150 K and with the earlier results of Heeger and collaborators.[19]

B. Anomalous electron-intramolecular-vibration coupling

The first-order coupling of the a_g modes to the CDW phase oscillation is not the only mechanism for EIMV coupling. This is clearly shown in the data of Figs. 4 and 5. The vibrational mode of interest has a primarily CN-stretching characteristic and is situated at about 2220 cm^{-1}. Figure 4 shows the temperature dependence of this structure which is the strongest normally IR-active mode in TTF-TCNQ. The main absorption of this structure is at 2216 cm^{-1} at room temperature. It corresponds to the two IR-active vi-

brational modes of the four CN groups; i.e., ν_{19} and ν_{33} both observed at 2228 cm^{-1} in $TCNQ^0$. In Fig. 10(a) we show the atomic and charge displacements associated with these modes. ν_{19} and ν_{33} correspond to oscillating dipoles along the long and short molecular axes, respectively. As the temperature is decreased below the Peierls transition ν_{19} appears to split off from ν_{33} and shift to lower frequencies. The temperature dependence of the splitting shown in Fig. 5 appears to follow closely that of the CDW amplitude.

The assignment of the two split modes to ν_{19} and ν_{33} is due to their polarization. Figure 10(b) shows the arrangement of the TCNQ stacks in TTF-TCNQ. It is seen that the dipole moment associated with ν_{19} mode has components along the b and c axes, while that of ν_{33} has a component along the a axis only. The polarized reflection data of the CN-stretching mode shown in Fig. 6 has been taken on a mosaic of TTF-TCNQ single crystals laid flat on their ab face with the incident light direction close to normal to the ab plane. The two polarizations $\vec{E} \parallel b$ and $\vec{E} \perp b$ ($\vec{E} \parallel a$), therefore, couple to the dipole moments of ν_{19} and ν_{33}, respectively. At room temperature the two modes appear to be degenerate. At $T = 20$ K the data shown in Fig. 6(b) clearly show that the mode shifted to the lower energy is ν_{19} which has a dipole polarized along the long axis of the molecule.

The anomalous result of the EIMV coupling to an asymmetric IR-active mode has not been considered in TTF-TCNQ or any of the other 1D organic semiconductors. The present result does indeed call for a new mechanism to explain such a coupling. The results of Fig. 3 indicate that such a coupling does not split the two modes symmetrically. Due to thermal stiffening of the modes in lowering the temperature, ν_{33} blue-shifts to 2222 cm^{-1} by about 6 cm^{-1} together with all the other IR-active modes. The splitting is then caused by the lowering of the frequency of ν_{19} by 6 cm^{-1}. The temperature dependence of the splitting shown in Fig. 5 clearly indicates that the frequency shift of ν_{19} is a result of its coupling to the CDW amplitude.

A strong coupling of ν_{19} to the CDW is expected if the Peierls distortion is a result of molecular motion in the bc plane (see Fig. 10). Such considerations as the position of CN groups at the four corners of the TCNQ molecules, a large density of unpaired π electrons on the CN groups, the close interchain separation of CN pairs on the neighboring TCNQ molecules, and the direction of polarizability associated with ν_{19} all tend to emphasize its coupling to a molecular motion in the bc plane. Such a motion has recently been found in the isostructural selenium analog of TTF-TCNQ, TSeF-TCNQ, which also shows a similar splitting of ν_{19} and ν_{33} modes with the onset of Peierls transition.[38] The detailed analysis of a recent x-ray diffuse scattering results indicates[39] that the Peierls distortion in TSeF-TCNQ appears to arise from a two-dimensional ordering of the donor and acceptor molecules in their respective sheets in a bc plane.[9] We note that although the detail of the molecular motion associated with the CDW in TTF-TCNQ is not established the distortion has primarily b and c components.[16]

We have also considered other mechanisms to explain the anomalous results of Figs. 4–6. An alternative possibility is that the splitting is caused by the vibronic structure of $a_g(Q_2)$ which has the right qualitative features. Such an assumption, however, would result in too small a value for λ_2. Further such a mode is expected to have a width of about $\lambda_2\omega_2^{\phi}$; i.e., $\delta\omega_2^{\phi} \simeq 60$ cm^{-1} which is an order of magnitude larger than that of the observed structure. The fact that the two absorptions have different polarizations rules out other possibilities such as band folding which should result in the appearance of new zone-center modes, asymmetric displacement of the unpaired electron on TCNQ and subsequent formation of the Wigner condensation on the TCNQ sublattice.[40]

The size of the splitting of ν_{19} mode from ν_{33} mode should in principle depend on the amplitude of the molecular displacement which is a measure of the CDW amplitude. Therefore, the temperature dependence of the splitting should follow that of the CDW amplitude. The similarity between the temperature dependence of the splitting (Fig. 5) and that of the intensity of the vibronic mode Fig. 3 supports this point of view. Due to the weak intensity of the vibronic structures in TTF-TCNQ, evaluation of the temperature dependence of the CDW amplitude through the measurement of the splitting is potentially more accurate. Whereas the strongest vibronic structure shown in Fig. 3 becomes undetectable above $\simeq 70$ K, the splitting shown in Fig. 5 is detectable for temperatures as high as about 150 K. The uncertainty in the magnitude of the splitting at higher temperatures arises primarily from the finite absorp-

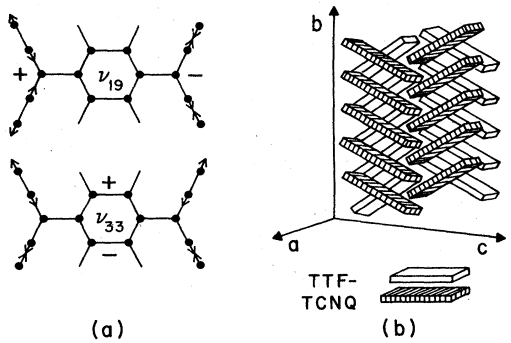

FIG. 10. (a) Atomic and charge displacement associated with IR-active modes of the CN-stretching vibration. (b) A perspective view of TCNQ stacking in TTF-TCNQ, adopted from R. Comes in Ref. 3.

tion width of microcrystalline samples dispersed in KBr pellets.

Besides the sharp structure associated with the CN-stretching mode at about 2220 cm^{-1} a broad absorption band is also observed at about 2050 cm^{-1} at room temperature (see Fig. 1). The position of this broad absorption band relative to the CN-stretching vibration region indicates that they are closely related. Figure 8 shows the polarized reflectivity result in the region of the CN-stretching vibration for several temperatures. The broad structure is primarily polarized parallel to the stacking axis and it is not observed for $T < 150$ K. We note the disappearance of this structure is concurrent with the onset of 1D order in TCNQ chains. The sizable integrated oscillator strength of this anomalous structure and the fact that it is polarized parallel to the stacking axis suggests that it is electronic in origin.

C. General discussions

The result of above discussion clearly indicates the intramolecular vibrations are strongly coupled to unpaired π electrons in TTF-TCNQ. As a result a study of the vibrational spectrum, in particular as a function of temperature, can be a powerful tool for probing the electronic as well as lattice dynamics of TTF-TCNQ. A study of the vibrational spectrum can be performed with relative ease using not so elaborate spectroscopic technique. The well-developed IR spectroscopy can in principle provide a different view of the electronic properties of organic solids such as TTF-TCNQ. The high resolution achieved in conventional IR spectroscopy in some respect can provide a more accurate description of the behavior of the π electrons, reflected in the microscopic structure of the intramolecular vibrations, than the conventional x-ray and/or neutron-diffraction spectroscopy. We have thus far discussed the behavior of electronic CDW as seen through the intramolecular vibrations, and the role that the sizable total EIMV coupling constant may play in stabilizing the Peierls distortion.

Based on the difference in the structure factor for neutron scattering of protonated and deuterated crystals, Carneiro[40] suggested that the Kohn anomaly in TTF-TCNQ occurs in CH- (or CD) stretching modes rather than in an acoustic phonon. The result of Fig. 7 shows that this cannot be the case. We do not observe any sudden change in the frequency or intensity of the CH-stretching modes at the transition temperature.

The nature of the ground state of TTF-TCNQ at low temperatures has also been a subject of considerable controversy. Based on the suggestion that the Coulomb correlation energy is larger than the bandwidth,[41] Yamaji has suggested that at $T=0$ TTF-TCNQ is in an antiferroelectrically ordered ground state.[42] In his model a Wigner crystal is formed by the unpaired electrons of the TCNQ sublattice. The electrons are then localized on two CN bonds at opposite ends of two $TCNQ^-$ neighbors which are separated by a $TCNQ^0$ along the stacks. If such a model were correct we should have seen two distinct sets of modes associated with $TCNQ^0$ and $TCNQ^-$ as the temperature is lowered below T_c. The experimental results presented in this work refute such a possibility.[42]

IV. SUMMARY AND CONCLUSION

We have presented the experimental evidence for electron-intramolecular-vibration coupling in TTF-TCNQ. Linear coupling of totally symmetric vibrations of the a_g modes to the oscillation in the phase of the CDW give rise to a set of vibronic modes which correspond to the bodily displacement of the CDW along the stacks. We have also discovered that some normally IR-active modes can couple to the CDW. Such a coupling is a result of the molecular displacement due to the onset of Peierls distortion. This coupling has been observed in the CN-stretching mode of TCNQ that is very sensitive to molecular motion in the *bc* plane.

The temperature dependence of the intensity of the vibronic modes, as well as the splitting of the CN-stretching mode caused by the molecular displacements, are used to monitor the growth of CDW in TTF-TCNQ with decreasing temperature. The intensity of the vibronic modes and the size of the splitting indicates the fluctuating CDW's in the range $53 < T < 150$ K have large amplitude. These results support the point of view that the collective contribution to the conductivity due to sliding CDW's is not limited to the region close to the transition at $T_{c1}=53$ K. We note that in contrast to the previously studied systems the low transition temperature in TTF-TCNQ provides a unique opportunity to study the temperature dependence of the CDW amplitude.

We have found that the dimensionless EIMV coupling constants for the a_g modes of the TCNQ molecule in TTF-TCNQ are in good agreement with their theoretical estimates, as well as the values obtained by extrapolating the result from previous studies. For our experimental determination of λ_n's we have derived an expression for the difference between the frequency of a vibronic mode and its unperturbed zone-center a_g mode. This expression valid in the limit of weak coupling is quite sensitive to the value of λ used as the single parameter for the fit. We have, therefore, obtained a value of $\lambda \simeq 0.35$ for the total electron-phonon coupling constant for the TCNQ stacks.

We have also pointed out the significance of the vibrational mode studies as a function of temperature in providing insight into the electronic properties and

lattice dynamics of organic solids. The attraction of such approach arises primarily from the relative ease that high-resolution IR spectroscopy can be performed.

ACKNOWLEDGMENTS

I would like to thank Dr. M. J. Rice for his interest in this work and for helpful communications. I am grateful to Professor Heeger for his hospitality during the time this manuscript was being prepared. Helpful discussions with Professor Heeger, Professor Pecile, and Professor Weger are acknowledged. I am indebted to Dr. E. M. Engler and Dr. J. B. Torrance for gifts of some of the samples. I thank Ms. A. Iraji-Zad and Mr. M. Mahdavi for their technical assistance. This work was in part supported by the grant (600-4-35/2) from the ministry of higher education.

---

*Present address: Dept. of Phys., Univ. of Pennsylvania, Philadelphia, Pa. 19104.
†Previously known as Arya-Mehr University of Technology.

[1] *Low-Dimensional Cooperative Phenomena,* edited by H. J. Keller (Plenum, New York, 1975).
[2] *Chemistry and Physics of One Dimensional Metals,* edited by H. J. Keller (Plenum, New York, 1977).
[3] *One Dimensional Conductors,* edited by J. T. Devreeze, R. P. Evrard, and V. E. van Doren (Plenum, New York, 1978).
[4] *Proceedings of the Dubrovnik Conference on Quasi One-Dimensional Conductors,* Lecture Notes in Physics, edited by S. Barisic (Springer-Verlag, New York, 1979), Vols. 96 and 97.
[5] R. E. Peierls, *Quantum Theory of Solids* (Oxford University Press, London, 1955), p. 108.
[6] D. Jerome, A. Mazaud, M. Ribault, and K. Bechgaard, J. Phys. (Paris) Lett. 41, L-95 (1980).
[7] T. J. Kistenmacher, T. E. Phillips, and D. O. Cowan, Acta Crystallogr. B 30, 763 (1974).
[8] M. J. Cohen, L. B. Coleman, A. F. Garito, and A. J. Heeger, Phys. Rev. B 13, 5111 (1976).
[9] S. Etemad, Phys. Rev. B 13, 2254 (1976).
[10] A. A. Bright, A. F. Garito, and A. J. Heeger, Phys. Rev. B 10, 1328 (1974).
[11] D. B. Tanner, C. S. Jacobson, A. F. Garito, and A. J. Heeger, Phys. Rev. B 13, 3381 (1976).
[12] P. M. Chaikin, J. F. Kwak, R. L. Greene, S. Etemad, and E. M. Engler, Solid State Commun. 19, 1201 (1976).
[13] S. Etemad, E. M. Engler, T. D. Schultz, T. Penney, and B. A. Scott, Phys. Rev. B 17, 513 (1978).
[14] S. Etemad, T. Penney, E. M. Engler, B. A. Scott, and P. E. Seiden, Phys. Rev. Lett. 34, 741 (1975).
[15] F. Denoyer, R. Comes, A. F. Garito, and A. J. Heeger, Phys. Rev. Lett. 35, 445 (1975); S. Kagoshima, H. Anzai, K. Kajimura, and T. Ishiguro, J. Phys. Soc. Jpn. 39, 1143 (1975).
[16] S. K. Khanna, J. P. Pouget, R. Comes, A. F. Garito, and A. J. Heeger, Phys. Rev. B 16, 1468 (1977); S. Kagoshima, T. Ishiguro, and H. Anzai, J. Phys. Soc. Jpn. 41, 2061 (1976).
[17] Y. Tomkiewicz, A. R. Taranko, and J. B. Torrence, Phys. Rev. Lett. 36, 751 (1976).
[18] J. E. Eldridge, Solid State Commun. 26, 243 (1978).
[19] A. J. Heeger, p. 69 in Ref. 3.
[20] A. Andrieux, H. J. Schulz, D. Jerome, and K. Bechgaard, Phys. Rev. Lett. 43, 227 (1979).
[21] M. J. Rice, N. O. Lipari, and C. B. Duke, Solid State Commun. 17, 1089 (1975).
[22] M. J. Rice and N. O. Lipari, Phys. Rev. Lett. 38, 437 (1977).
[23] M. J. Rice, L. Pietronero, and P. Bruesch, Solid State Commun. 21, 757 (1977).
[24] M. J. Rice, N. O. Lipari, and S. Strassler, Phys. Rev. Lett. 39, 1359 (1977).
[25] M. J. Rice, V. M. Yartsev, and C. S. Jacobson, Phys. Rev. B 21, 3437 (1980).
[26] M. J. Rice, Phys. Rev. Lett. 37, 36 (1976).
[27] N. O. Lipari, M. J. Rice, C. B. Duke, R. Bozio, A. Girlando, and C. Pecile, Int. J. Quantum Chem. 11, 583 (1977).
[28] W. T. Wozniak, G. Depasquali, M. V. Klein, R. L. Sweany, and T. L. Brown, Chem. Phys. Lett. 33, 33 (1975). As pointed out by the authors their results were dominated by the effect of neutral TTF and TCNQ molecules present in their samples.
[29] C. Benoit, M. Galtier, A. Montaner, J. Deumie, H. Robert, and J. M. Faber, Solid State Commun. 20, 257 (1976). Their IR spectra are quite uncharacteristic of TTF-TCNQ. We note that the strong absorption due to the CN-stretching mode of vibration is conspicuously absent in their spectra.
[30] E. Aharon-Shalom, M. Weger, I. Agranat, and E. Wiener-Aonear, Solid State Commun. 23, 53 (1977). The authors present room-temperature IR spectra that are polarized perpendicular to the stacking b axis. Besides the absence of CDW at $t = 300$ K their spectra have the wrong polarization to show the EIMV coupling.
[31] These Fano-type interference structures [U. Fano, Phys. Rev. 124, 1866 (1961)] appear as indentations in the continuum background of frequency-dependent conductivity; see the effect of the CN-stretching mode in TEA$(TCNQ)_2$ in Ref. 23.
[32] H. Temkin and D. B. Fitchen, in *Proceedings of the International Conference on Lattice Dynamics,* edited by M. Balkansky (Flammarion Sciences, Paris, 1977), p. 587.
[33] Kuzmany and H. J. Stolz J. Phys. C 10, 2241 (1977).
[34] R. Comes, S. M. Shapiro, G. Shirani, A. F. Garito, and A. J. Heeger, Phys. Rev. B 14, 2376 (1976).
[35] H. Gutfreund, B. Horovitz, and M. Weger, J. Phys. C 7, 383 (1974).
[36] B. Horovitz, H. Gutfreund, and M. Weger, Phys. Rev. B 17, 2796 (1978).
[37] P. Bak and V. J. Emery, Phys. Rev. Lett. 36, 978 (1976).
[38] S. Etemad (unpublished results).
[39] R. Comes and K. Yamaji (private communication).
[40] K. Carneiro, Phys. Rev. Lett. 37, 1227 (1976).
[41] J. B. Torrance, in Ref. 2, p. 137.
[42] K. Yamaji, Solid State Commun. 27, 425 (1978).